Chem Soc Rev

This article was published as part of the

In-situ characterization of heterogeneous catalysts themed issue

Guest editor Bert M. Weckhuysen

Please take a look at the issue 12 2010 table of contents to access other reviews in this themed issue

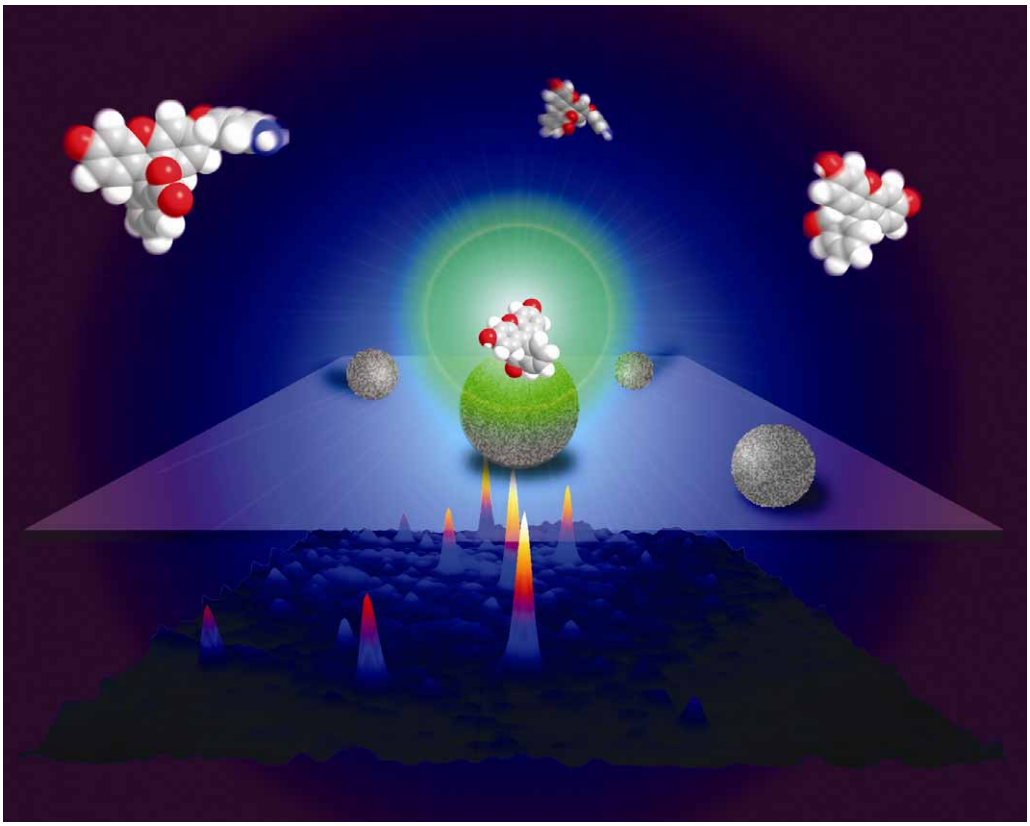

Exploring catalytic solid/liquid interfaces by *in situ* attenuated total reflection infrared spectroscopy†

Jean-Michel Andanson and Alfons Baiker*

Received 4th June 2010
DOI: 10.1039/b919544k

In situ attenuated total reflection Fourier transform infrared (ATR-FT-IR) spectroscopy has gained considerable attention as a powerful tool for exploring processes occurring at solid/liquid and solid/liquid/gas interfaces as encountered in heterogeneous catalysis and electrochemistry. Understanding of the molecular interactions occurring at the surface of a catalyst is not only of fundamental interest but constitutes the basis for a rational design of heterogeneous catalytic systems. Infrared spectroscopy has the exceptional advantage to provide information about structure and environment of molecules. In the last decade, *in situ* ATR-FT-IR has been developed rapidly and successfully applied for unraveling processes occurring at solid/liquid interfaces. Additionally, the kinetics of complex reactions can be followed by quantifying the concentration of products and reactants simultaneously in a non-destructive way. In this *tutorial review* we discuss some key aspects which have to be taken into account for successful application of *in situ* ATR-FT-IR to examine solid/liquid catalytic interfaces, including different experimental aspects concerned with the internal reflection element, catalyst deposition, cell design, and advanced experimental methods and spectrum analysis. Some of these aspects are illustrated using recent examples from our research. Finally, the potential and some limitations of ATR will be elucidated.

1. Introduction

In heterogeneous catalysis reactants and catalyst are present in different phases, and the reaction typically takes place at solid/gas, solid/liquid, or solid/liquid/gas interfaces. For designing new efficient catalysts and for optimizing catalytic processes

Institute for Chemical and Bioengineering, Department of Chemistry and Applied Biosciences, ETH Zurich, Hönggerberg, HCI, CH-8093 Zürich, Switzerland. E-mail: baiker@chem.ethz.ch
† Part of the themed issue covering recent advances in the *in-situ* characterization of heterogeneous catalysts.

Jean-Michel Andanson

Jean-Michel Andanson was born in Clermont-Ferrand (France) in 1976 and received his Doctorate degree in physical-chemistry from the University of Bordeaux in 2005. During his PhD he investigated the structure, properties, and specific molecular interactions of supercritical fluids using vibrational spectroscopy and molecular dynamics simulations under the supervision of Prof. Marcel Besnard and Jean-Christophe Soetens. From 2006 to 2008, he was a postdoctoral associate of Prof. Sergei G. Kazarian in Imperial College London (U.K.). Then, he joined the group of Prof. Alfons Baiker at ETH Zürich (Switzerland) to work with infrared and Raman spectroscopy on ionic liquids—supercritical carbon dioxide biphasic systems.

Alfons Baiker

Alfons Baiker studied chemical engineering at ETH Zurich and earned his PhD degree in 1974. After several post-doctoral stays at different universities he finished his habilitation at Stanford University (California) and returned to ETH in 1980, where he started his own research group focusing on heterogeneous catalysis and reaction engineering at the Department of Chemistry and Applied Biosciences. He moved up to the ranks to become Full Professor in 1990. His research interests, documented in more than 830 publications in refereed journals and numerous patents, are centered around catalyst design and novel catalytic materials, mechanisms and kinetics of catalytic surface processes, asymmetric hydrogenation, selective oxidation, environmental catalysis, chiral surfaces, in situ spectroscopy, and the application of supercritical fluids in catalysis. His goal is to further the scientific basis needed for developing environmentally-benign chemical processes which make optimal use of raw materials and energy.

understanding of the behavior of the different components of the system under reaction conditions, that is *in situ*, is essential. Since the pioneering work of Eischens and coworkers[1,2] in the fifties of the past century, *in situ* infrared spectroscopy has developed to an indispensable tool in catalysis research, where the elucidation of the relationship between the structural and chemical properties of a catalytic interface (surface) and its catalytic performance is of prime interest. Knowledge of this structure–activity relationship not only allows optimizing the performance of a catalyst but also provides crucial information for the rational design of new more efficient catalytic materials. Among the various spectroscopic methods[3] applied for monitoring reactions and catalytic interfaces under working conditions, that is under *operando* conditions, infrared and Raman spectroscopy are most frequently applied. An infrared technique particularly suitable for the *in situ* investigation of solid/liquid and solid/liquid/gas interfaces is attenuated total reflection Fourier transform infrared spectroscopy (ATR-FT-IR).

This tutorial review is mainly based on the experience we have gained in our laboratory over more than a decade of using ATR-FT-IR spectroscopy for the elucidation of catalytic solid/liquid and solid/liquid/gas interfaces. For a detailed consideration of ATR-FT-IR the reader is referred to previous comprehensive reviews[4–6] and books.[7–9]

Vibrational (infrared or Raman) spectroscopy of molecules adsorbed on the catalyst surface provides information about the molecular orientation and interaction, as part of the vibrational spectrum is sensitive to the environment, and consequently the spectrum of a molecule dissolved in a solvent is different to that of the same molecule adsorbed on a surface. Both intra- and inter-molecular interactions can be detected and, as infrared and Raman spectroscopy are probing molecular vibrations, these spectroscopies can be used to analyze which atom is interacting with the surface and what is the orientation of the adsorbed molecule. In practice, the detailed analysis of a spectrum can be difficult, and to discriminate among the molecules those which are of interest for understanding the catalytic system is often challenging.

ATR-FT-IR spectroscopy has, compared to the usual transmission FT-IR spectroscopy, the advantage that it probes only molecules which are located on the surface and in the surface near region of the sample. Fig. 1 presents schematically different infrared spectroscopy modes; in transmission mode the light passes through the whole sample while in the ATR approach the light is reflected on the surface and only molecules located in the first (few) micrometre(s) over the surface of the internal reflection element (IRE) are interacting with the infrared light.

In practice, FT-IR spectroscopy in transmission mode appears to be rather limited for investigating solid/liquid interfaces, as the IR light is already strongly absorbed within only a few micrometres of path into liquid or solid samples. In the past decades, the utilization of the ATR approach has gained increasing attention, at first mainly in electrochemistry[10–12] and later in heterogeneous catalysis[13–18] among many other applications.

In this tutorial review we aim at providing the reader a practitioner's view on *in situ* ATR-FT-IR spectroscopy and discuss some crucial experimental aspects, including cell design and experimental methodologies. Finally, a series of case studies which emerged from our laboratory in the past decade are used for illustrating the potential and limitation of the technique.

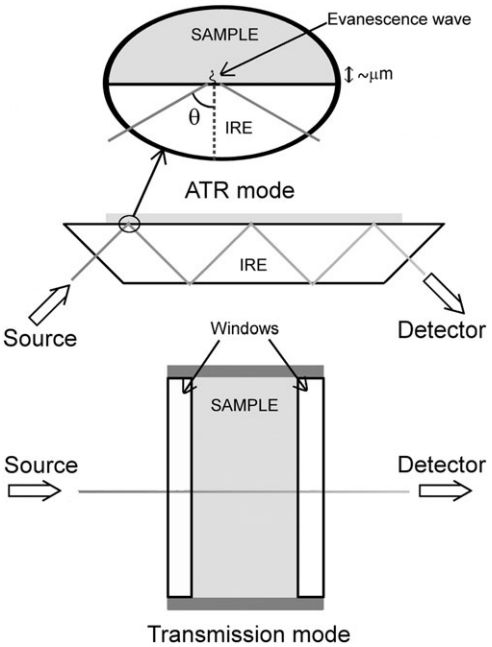

Fig. 1 Principle path of IR-beam in transmission IR and ATR-IR.

2. Fundamental aspects

Harrick[19] and Fahrenfort[20] established infrared internal reflection spectroscopy half a century ago. In the ATR-FT-IR technique (Fig. 1), the beam of infrared radiation traverses a crystal of relatively high refractive index (called internal reflection element (IRE)) and hits the crystal surface at an angle of incidence, θ, greater than the critical angle (θ_{crit}):

$$\theta_{crit} = \sin^{-1}(n_s/n_c) \quad (1)$$

where n_s and n_c are the refractive indices of the sample and the crystal, respectively. The angle of incidence is defined as the angle between the incident light and the perpendicular of the interface between the IRE and the sample. As explained by Maxwell's theory, under such conditions light is reflected at the interface and forms an evanescent wave perpendicular to the total reflecting surface. If the sample absorbs a fraction of this radiation, the propagating wave interacts with the sample and becomes attenuated, giving rise to a reflection spectrum, similar to the absorption spectrum. The intensity of the evanescent electric field penetrating into the sample undergoes an exponential decay:

$$E = E_0 e^{(-z/d_p)} \quad (2)$$

where E is the electric field amplitude at a penetration distance z, E_0 is the electric field amplitude at the interface, and d_p is the penetration depth given by:

$$d_p = \frac{\lambda}{2\pi\sqrt{(n_1^2 \sin^2\theta - n_2^2)}} \quad (3)$$

where λ is the wavelength of the incident beam, θ is the incident angle, n_1 is the refractive index of the IRE and n_2 is the refractive index of the sample. To compare ATR and transmission spectra, the effective thickness (d_e) can be used which expresses the equivalent path length in a hypothetical transmission measurement yielding the same absorption as in an ATR experiment.

$$d_e = \frac{n_2/n_1 E_0^2 d_p}{2 \cos \theta} \quad (4)$$

ATR infrared spectroscopy allows us to measure an infrared spectrum equivalent to a very short transmission cell as both d_p and d_e are on the scale of a micrometre. A general difficulty of ATR-FT-IR measurements is the need of good and uniform contact of the sample with the IRE, as will be discussed in Section 3.2.

3. Internal reflection element (IRE)

3.1 Material

The choice of the IRE material is important as the crystal will be in contact with the sample during the experiment and most of the materials show certain limitations. First of all, the material must be transparent in the IR range (4000–400 cm^{-1} for middle IR radiation, generally being used for ATR). A list of some materials used as IRE, their refractive indices and main limitations are given in Table 1. Diamond for instance is slightly absorbing in the range of 2400–1900 cm^{-1}; but only a few bands of interest are in this range (mainly some CO and CN stretching bands). For other spectral ranges, diamond can be used without limitation even in a multiple reflections setup, which is possible even with a small crystal.[21] Despite its relatively high price, diamond has the advantage of being more mechanically robust and chemically stable than other IRE materials.

A crucial property of the IRE is the refractive index which must also be selected carefully as the quality of the ATR-FT-IR spectrum will depend on it. In Table 2 the effective thicknesses (d_e in eqn (4)) for several usual arrangements are listed. The increase of the refractive index of the IRE from 2.42 (ZnSe or diamond) to 4.0 (Ge) induces a decrease of 85% of the effective thickness (with refractive index of the sample 1.5 and incident angle of 45°) which will strongly reduce the absorbance of the sample, and thus the signal-to-noise ratio (S/N). Another factor to be considered in the choice of the IRE crystal is the absorptivity of the sample. A common problem encountered in ATR-FT-IR is its restriction to incident angles greater than the critical angle. When the refractive index of the sample is high (>1.6) using ZnSe with an incident angle of 45° becomes inappropriate. As an example, Al_2O_3 has a refractive index of 1.6 to 1.8 (with metal dispersed in it as for example in an alumina supported metal catalyst, the refractive index is increased). Even if the incident angle is slightly lower than the critical angle, it is not recommended to utilize such a setup, as the IR spectrum will most probably be distorted (as the refractive index of the powder is not constant and can locally change). To overcome this problem, the incident angle (generally to 60°) or the refractive index of the IRE (usually by using Ge) can be increased. A Ge crystal with a 60° incident angle will be necessary for investigating a sample like TiO_2 (rutile) with a refractive index of 2.6–2.7.

Table 1 IRE materials commonly used for ATR and some of their properties

Material	Refractive index	Potential limitations
Diamond (C)	2.42	Expensive
Germanium (Ge)	4.0	Fragile, max. 125 °C
KSR-5 (thallium bromo-iodide)	2.35	Fragile, toxic, slightly soluble in water, soluble in bases
Silicon (Si)	3.45	Not transparent below 1500 cm^{-1}, unsuitable for pH above 12
Zinc selenide (ZnSe)	2.42	Suitable only for pH between 5 and 9
Zinc sulfide	2.2	Unsuitable for strong acids and bases

Table 2 Examples of penetration depth and effective thickness for different IRE materials (refractive indices of ZnSe and Ge are 2.42 and 4.0, respectively), incident angles, wavenumber and refractive indices of the investigated samples

Material	Incident angle/°	Wavenumber/cm^{-1}	Refractive index of the sample	Penetration depth/μm	Effective thickness/μm
ZnSe	**45**	**1000**	**1.5**	1.933	4.126
ZnSe	45	1000	**1.1**	1.214	1.476
ZnSe	45	1000	**1.3**	1.430	2.291
ZnSe	45	1000	**1.7**	8.1	24
ZnSe	45	1000	**1.71**	25	75
ZnSe	45	**4000**	1.5	0.483	1.032
ZnSe	45	**2000**	1.5	0.966	2.063
ZnSe	**60**	1000	1.5	1.087	1.481
ZnSe	**60**	1000	**1.7**	1.298	2.347
Ge	45	1000	1.5	0.664	0.614
Ge	45	1000	**1.7**	0.704	0.775
Ge	**60**	1000	1.5	0.510	0.323

3.2 Catalyst deposition

Catalysts are usually deposited in two forms on IRE; as films (*e.g.* metal film) which must be thinner than the evanescence electric field which is probing adsorbed molecules at the outer interface of the model catalyst, or as layers of powders which can be much thicker because molecules can penetrate into the deposited layers through inter- and intra-particle void space (Fig. 3).

3.2.1 Thin metal film. A thin metal film (*e.g.* gold, silver, platinum *etc.*) is easily prepared by physical vapor deposition (PVD) techniques directly on the IRE.[22] The thickness of the film must be thinner than the penetration depth of the evanescent wave at any wavelength of interest. The metal film is generally optimal with a thickness of a few nanometres. PVD techniques are nowadays broadly used and a detailed discussion of the optimization of metal films can be found in an earlier review.[4]

3.2.2 Powder catalyst. The deposition of a catalyst on the IRE can be accomplished using several different methods. In the simplest cases it can be achieved by dropping a slurry (*i.e.* a highly concentrated suspension) of the catalyst onto the IRE followed by drying (*e.g.* for a few hours at 80 °C). Examples where this method has been applied include Al_2O_3,[23] TiO_2,[24] modified silica,[25] and CeO_2.[26] These deposited layers are normally mechanically not very stable, but usually possess sufficient stability to resist the shear tension created by a flowing solvent for hours. The durability of the layer depends mainly on the catalyst, the IRE material, preparation conditions, flow rate and solvent. As an example, a 5 wt% Pd/Al_2O_3 layer coated over ZnSe is shown in Fig. 2. In cases where it is not possible for a specific application to deposit a durable layer with this simple direct dropping technique, the powder particles can be attached to the IRE using a binder material which is coated first on the IRE.[27,28]

Note that the catalyst immobilized on the IRE is often not present as a homogeneous layer perfectly in contact with the IRE, and consequently the evanescent field is not exactly created as described by theory (eqn (3)). The advantage of using a powder with small particles is to provide good sensitivity for spectra of adsorbed species as the surface area increases thereby, so does the number of molecules probed by the ATR evanescent wave compared to a thin film. A problem encountered by depositing a powder consisting of nanoparticles smaller than the penetration depth is the structural complexity of the resulting particle layer. The evanescence wave is probing catalyst particles, together with empty space between the particles. During an *in situ* experiment, the space between the particles is filled by the fluid consisting of reactant(s), product(s), and solvent, as illustrated in Fig. 3. In a heterogeneous material, when particles (or pores) are much smaller than the penetration depth, the refractive index can be approximated by:

$$n_{\text{eff}} = \sqrt{(1-\Phi)n_1^2 + \Phi n_p^2} \qquad (5)$$

where Φ is the volume of the small pores, and n_1 and n_p are the refractive indices of the continuous and dispersed phases, respectively.[30]

To calculate accurately the penetration depth of the evanescent wave, detailed knowledge of the catalyst layer is necessary. If such information is not accessible, quantitative data become difficult to extract. Nevertheless, if reproducibility of the data is achievable, a comparison between data collected at different conditions becomes feasible. For illustration, the volume of the pores can easily be around 50%, which in the case of Al_2O_3 would decrease the refractive index from 1.7 to 1.4 (when pores are filled with air). On the other hand, 5 wt% of metal in Al_2O_3 will only increase the refractive index by 2 to 3%.

A practical way for increasing the effective thickness (and thus improving the signal/noise ratio) without getting too close to the critical angle is the utilization of several active reflections. Many available ATR cells have optics which create

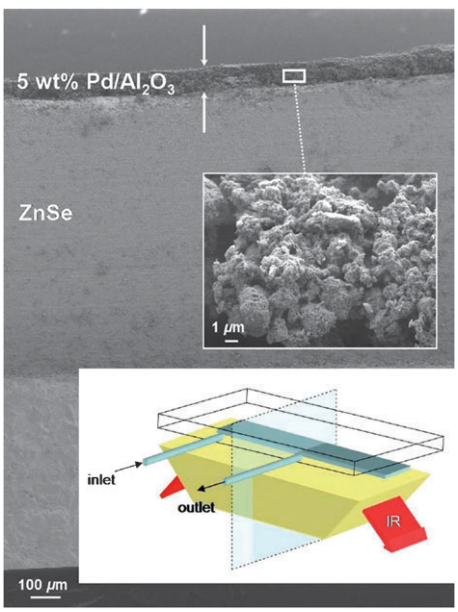

Fig. 2 Scanning electron microscopic (SEM) image of the ZnSe internal reflection element coated with a layer of 5 wt% Pd/Al_2O_3. The inset shows the porous structure of the catalyst. A drawing of the ATR reactor cell is also shown with the cross section along which the SEM image was taken (reprinted from ref. 29. Copyright 2005, with permission from Elsevier).

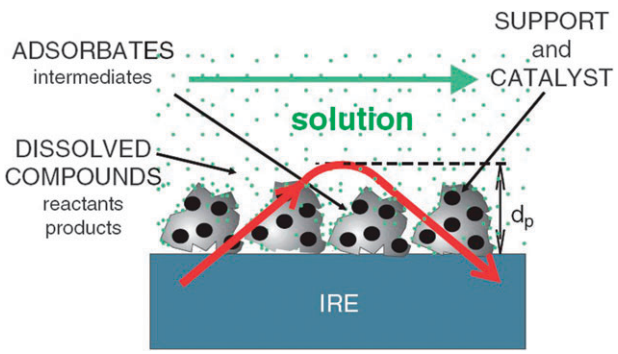

Fig. 3 *In situ* ATR-FT-IR spectroscopy of heterogeneous solid–liquid catalytic reactions gives simultaneous information about dissolved species and species adsorbed on the catalyst (reprinted from ref. 4. Copyright 2006, with permission from Elsevier).

up to 10 or even 25 active reflections. As seen from the examples shown below, the signal from molecules at the solid/liquid interface is generally fairly small (in the range of 1 mA (milli-absorbance) or lower), and the typical noise level of most experimental setups is not much smaller. As a consequence the noise must be reduced as much as possible; this is achieved *e.g.* by proper temperature control of the cell, avoidance of any movement of the cell, and a constant purging of the spectrometer. One should also be aware that in case of metallic nanoparticles or films, a possible enhancement of the IR signal around the metal is possible. The light-absorption properties were found to be changed dramatically by the mere presence of rough metal surfaces.[31] For IR quantitative analyses the possibility of surface-enhanced infrared absorption (SEIRA) should be carefully investigated, even in the case of a low concentration of metal, as the enhancement factor can be up to three orders of magnitude. Also when using thin metal films, SEIRA needs to be considered cautiously, as the surface corrugation of the film (nanometre scale) can change drastically the enhancement factor.

4. Cells

Nowadays, ATR cells are supplied by many companies around the world. As the ATR element is directly in contact with the components (solid/liquid/gas) of the investigated catalytic system it should be made of chemically resistant and mechanically durable materials. Specific setups have been developed for a wide range of applications, including high pressure, high and low temperature, or small volume (microfluidic) devices. Some special cells with variable incident angle, batch and continuous flow operation mode, multiple reflections (up to 25), or immersion probe have been developed and are nowadays used for both research and industrial applications (such as on-stream monitoring).

4.1 Batch cells

As an example of an ATR batch cell, a unit with modular components (including task-specific modifications of earlier versions) developed in our group is described in this paragraph. This cell is equipped with a horizontal ATR crystal (ZnSe or Ge; size 50 mm × 20 mm × 2 mm; angle of incidence 60°) as depicted in Fig. 4. In this specific arrangement, the active reflections are probing the bottom of the stainless steel cells. Sealing of the cell is accomplished using several Viton® O-rings connecting the modular parts.

The cell was upgraded recently for application with magnetic nanoparticles by adding a mechanical stirrer from top which replaced the original magnetic stirring system.[32] The cylindrical cell body (17.3 mL internal volume) is equipped with a mechanical axial flow impeller (diameter = 2.15 cm, Buchi Glas Uster AG). In this cell, most of the ATR crystal is not in contact with the sample, and only two active reflections are probing the material on the bottom of the cell, but the cylindrical shape of the internal volume of the cell allows a much more efficient mixing which is crucial for applications where mass transfer limitations are critical.

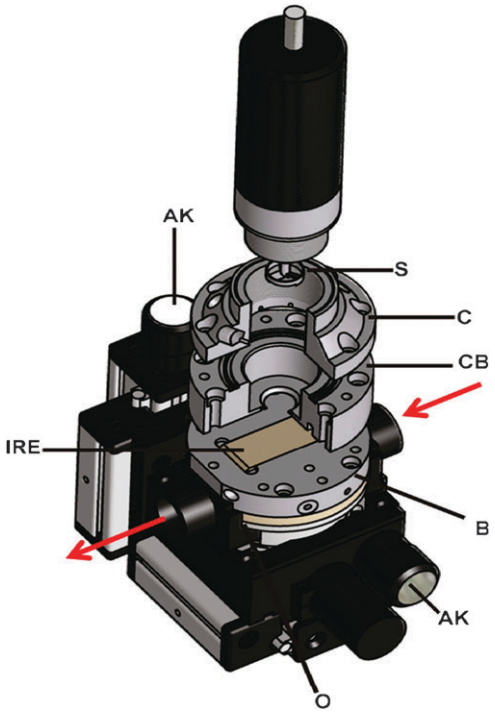

Fig. 4 Schematic view of the *in situ* reactor cell which is mounted within the sample compartment of the FT-IR spectrometer. S, mechanical stirrer; C, stainless steel cap; CB, stainless steel cell body; B, heatable base; O, optics; AK, horizontal and vertical adjusting knobs. The arrows represent the optical path of the IR radiation (reprinted with permission from ref. 32. Copyright 2009, American Chemical Society).

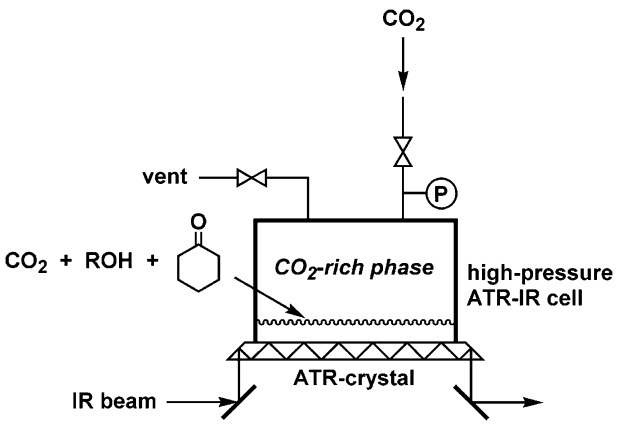

Fig. 5 High pressure ATR cell with six active reflections (adapted with permission from ref. 34).

4.2 High pressure batch cells

A high pressure cell was designed and built on the same base plate as the batch cell presented above, containing an internal volume of 10 mL (with essentially parallelepipedic shape above the ATR crystal), six active reflections, and magnetic stirring system. The cell can be used up to 120 °C and was tested up to 150 bar with a ZnSe crystal as IRE. The setup is schematically shown in Fig. 5. To prevent leakages even under high pressure, a Viton® O-ring is placed between the stainless

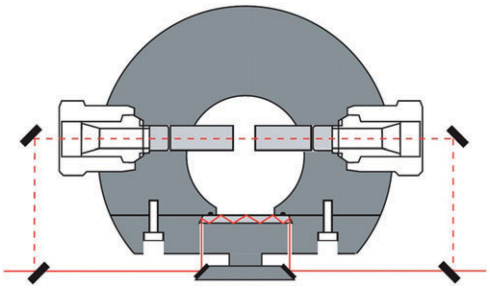

Fig. 6 Cross-section of the view-cell at the spectroscopic measurement level. The light beam is directed either through the ATR crystal or through the transmission windows. The four mirrors are mounted on a motor-driven mobile attachment. The cylindrical ZnSe windows, the additional cylinders to adjust the transmission path length, and the trapezoidal IRE are colored in light gray (reprinted with permission from ref. 35. Copyright 2003, American Institute of Physics).

steel and the IRE. To avoid any IR signal from the O-ring area, the optical arrangement of the high pressure cell (with the short side of the IRE in contact with the sample) should have the first active reflection far enough from the edge of the crystal. More details on this cell can be found in ref. 33.

When multiphase systems are studied, the quantification of species in each phase is often crucial for gaining a better understanding of the catalytic process. For this purpose another reactor cell was developed which facilitates *in situ* investigations of multiphase systems under high pressure by combining both transmission and ATR modes. A scheme of this high pressure cell is shown in Fig. 6. ATR-FT-IR measurements are realized using an IRE with three active reflections (27.7 × 10 × 2 mm, angle of incidence 60°, material used ZnSe or Ge), while the transmission measurements are done using two cylindrical windows in the upper part of the reactor. The transmission path length can be varied between 0.3 and 38 mm by adding supplementary crystals between the two windows of the transmission path. Special care is needed when working with the additional crystals inside the cell because of their brittleness. The four mirrors can be moved to enable the desired IR measurement mode. Moreover, the front of the cell has a sapphire window of 26 mm diameter which allows observing the inside of the cell (for phase behavior experiments) or to place a Raman probe which can be moved from one phase to the other. The light used to illuminate the inside of the cell was originally mounted at the back, but later at the front end of the cell because this arrangement resulted in improved visibility of the cell's content. The cell allows experiments at temperatures up to 200 °C and pressures up to 200 bar and the volume can be varied between 19.5 and 67.5 mL. More details of the setup are reported elsewhere.[35]

4.3 Continuous flow cells

A home-built stainless steel flow cell with small volume and rounded edges to avoid stagnant liquid during the flow experiments was used for *in situ* ATR-FT-IR studies. The flow cell can be heated and cooled by means of a thermostat. Liquids can be forced to flow over the sample by means of a peristaltic pump. The typical setup is presented in Fig. 7.

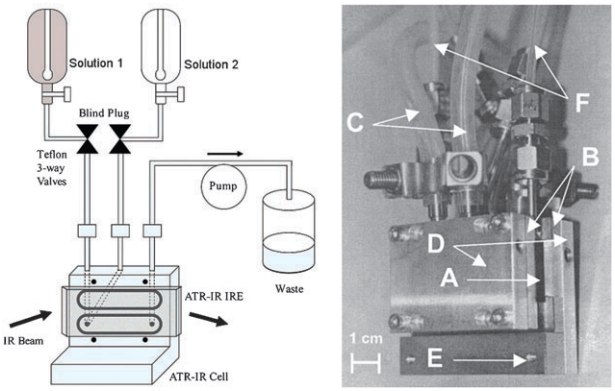

Fig. 7 (left) Schematic drawing and description of a flow cell and experimental setup (adapted with permission from ref. 36. Copyright 2003 American Chemical Society). (right) The home-built ATR flow cell used for *in situ* studies. The picture shows the cell body (A) together with a Ge IRE (B) and the cooling system (C, water tubings and D, cooling jackets). E points to the location of the thermocouple. F is the in- and outlet for the probing solution to and from the cell (reproduced with permission from ref. 37. Copyright Wiley-VCH Verlag GmbH & Co. KGaA).

The setup allows the modulation of the concentration of the liquid components in the feed by alternate opening and closing of the two valves.

4.4 Cells with fiber optics—immersion cells

Immersion cells have the advantage that they can be placed inside the reactor volume and thus allow probing the reactor content without the constraints imposed by the geometrical construction of the previous cells. An example of a setup based on an immersion cell is shown in Fig. 8. This cell type is particularly useful to follow reaction kinetics, as demonstrated for the catalytic esterification of 1-octanol and hexanoic acid over a Nafion/silica catalyst.[38] The monitoring of the reaction using ATR-FT-IR spectroscopy was validated by an off-line analysis using gas chromatography. Despite the catalyst not being deposited on the IRE, statistically a small proportion of the catalytic particles can still be observed in the IR spectrum. Using this experimental setup, *in situ* ATR-FT-IR has been successfully applied to detect the reaction of octanol with Si–O–H groups on SiO_2 particles during the catalytic esterification of octanol. Using such a setup, attention has to be given to the possibility that catalyst powder agglomerates on the IRE surface. A critical discussion of these cells for application in multiphase reactions has been given by Mul *et al.*[38] Using a bottom-mounted ATR setup, the risk of having particles accumulated on the bottom of the cell because of gravitational effects cannot be ignored. It can lead to overestimation of the observed reaction rates measured by ATR-FT-IR, particularly when using a cell with a small cavity on the bottom for placing the IRE, as has been discussed recently.[39] A representative example of the application of a fiber-optic coupled with ATR-FT-IR-probe for kinetic measurements has been reported for the reaction of phenyl isocyanate and phenol to diphenyl urethane in chloroform solution. An advantageous feature of this technique is that the kinetics of a reaction can be followed using IR spectroscopy without disturbing the system by taking

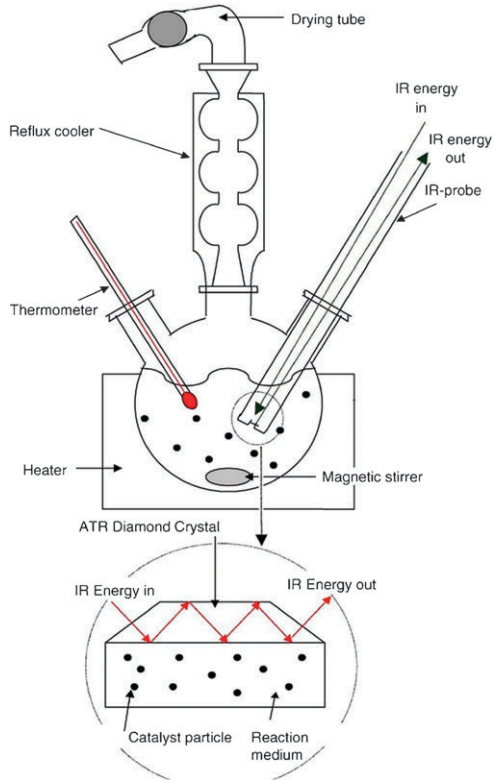

Fig. 8 ATR immersion cells with three active reflections in a reflux set-up (reproduced from ref. 38. Copyright (2004), with permission from Elsevier).

samples from the reactor. For studies where the goal is to measure the kinetics and not the investigation of the molecular interactions occurring at the solid/liquid interface, the immersion cells should be considered as the preferred choice.

Monitoring *in situ* the kinetics of a catalytic system is an important application in industry and many cells were developed for this purpose. Probes with multiple active reflections using small diamond ATR crystals have been under intensive development as diamond is chemically and mechanically resistant to most environments.[21]

5. Spectrum analysis and advanced experimental methods

5.1. Theoretical calculation of spectra

While *in situ* spectroscopic studies are normally performed under reaction conditions or conditions close to them, theoretical calculations of spectra frequently cannot account for such conditions and have to be drastically idealized and simplified. Nevertheless, nowadays density functional theory (DFT) calculations can be used to predict physical properties, including structure and vibrational spectra of a wide range of chemical systems. A typical calculation of an IR spectrum can be completed on a single molecule, on a molecular cluster or even on a molecule adsorbed on a nanoparticle using DFT.[40,41] As an example, several configurations (flat and tilted geometries) of the quinoline adsorption on the metal surface of a cluster of 31 atoms of Pt and Au have been calculated.[41] Even the simulation of such small model systems, which cannot completely mimic a real catalytic system, can greatly help in spectra analysis. The molecular structure and interactions indicated by the experimental IR spectra can be validated using computational studies which add considerable further credibility to spectra interpretation.

As an example, the vibrational modes of trifluoro-acetate adsorbed on Au (111), (100) and (110) surfaces were calculated for several conformations. The OCO symmetric and asymmetric stretching mode bands are red- and blue-shifted, respectively, while going from bidentate to unidentate in both calculated and experimental spectra.[42]

5.2 Greenler's surface selection rule

The infrared spectrum of an adsorbed molecule is normally not identical to the spectrum of the same molecule in the liquid phase. As already mentioned, specific molecular interactions are changing the IR spectrum. Furthermore, in case of the adsorption on a metal surface, the corresponding IR spectrum behaves according to the "metal-surface selection rules" developed by Greenler.[43,44] Because the electric field E (in eqn (2) and (4)) is always perpendicular to the surface of a perfect conductor (as a metal), a molecular vibration which does not induce a variation in the dipole moment with a component perpendicular to the surface of the metal will not absorb any IR light. In other words, depending on the orientation of the dynamic dipole moment of a vibration, some IR signals will be enhanced (vibrations with a dynamic dipole moment mainly perpendicular to the surface) while others will be diminished (vibrations with a dynamic dipole moment essentially parallel to the surface). As a result of this, the surface selection rule allows achieving a considerable further insight into the adsorption mode (orientation) of the adsorbed species.

As already introduced in the previous subsection, the adsorption of fluoro-acetate anions on a gold electrode has been recently studied using DFT calculations accompanied by ATR-FT-IR spectroscopy.[42] The computation predicts that the OCO asymmetric stretching band should be around 1670 cm^{-1}, while the experiment does not show any band in this region. For this vibration, the dynamic dipole is parallel to the metal surface, and hence the surface selection rule explains why this band is not observed experimentally.

5.3 Multivariate analysis

For chemical processes involving many components, the spectra collected do not always allow a simple analysis; in many cases a band does not correspond only to one component but contains contributions from several vibrations (also of different molecules). In the case of such a crowded spectrum the quantification of the reaction products by a simple univariate analysis (*e.g.* the intensity of one single wavenumber of the spectrum or the intensity of one specific band corresponding to one specific vibration) is frequently problematic. For quantifying certain species using bands of the IR spectrum, it is however possible to use a multivariate analysis. This is achieved by using more than one single band at a time, for example, a range [1800–1000 cm^{-1}] or even the total range of

the IR spectrum.[45,46] Various models have been developed for a variety of analytical chemistry applications including catalytic processes. Essentially, models can be classified in: (i) systems where all compounds are well known and the spectrum of each compound can be used as an input for the model, and (ii) systems where this information is not completely available.

In catalytic studies, the IR spectrum of each component is frequently known and even calibrations using several known solutions of the system can be done. In such situations the multivariate analysis can be approached as multiple linear regression, where the spectrum is the summation of the individual spectra weighed by their relative concentrations. As an example, the hydrogenation of acetophenone catalyzed by ionic liquid-stabilized rhodium nanoparticles was followed using a simple deconvolution of several ranges of the IR spectra.[47] Two models were developed, using different parts of the IR spectrum, to deconvolute the spectrum by the individual spectra of the main components of the reaction mixture. To improve the signal to noise ratio, the dataset used for analysis was obtained *via* the subtraction of two successive spectra measured during the reaction. Using the online analysis, the physical parameters (pressure, temperature) of the hydrogenation were optimized and selective hydrogenation reactions were thus obtained.[48] When some IR spectra are unknown, PCA (principal components analysis)-based methods can be used.[45] In this case it is necessary to make an estimation of the number of significant components to characterize all the possible mixtures.

5.4 Modulation excitation spectroscopy

Modulation excitation spectroscopy (MES) combined with phase sensitive detection (PSD) is a powerful method to enhance the sensitivity and discriminate between active and spectator species taking part in the investigated process. When a system is perturbed periodically by varying an external parameter (temperature, concentration, pressure, radiation (photocatalysis, microwave), pH, electric field, *etc.*) all the species of the system perturbed directly or indirectly by this parameter fluctuate with the same periodicity. Since only the responses to the excitation which are on the same time scale as the modulation can be observed in a modulation experiment, the frequency of the oscillation is an essential parameter which should be chosen carefully. Fig. 9 illustrates the features of a typical modulation excitation experiment with sinusoidal excitation (sin (ωt)). The IR signals corresponding to the active species (involved in the specific process) oscillate with the same frequency as the excitation, but with probably a certain phase delay and a non-linear response. Since the IR signals of the spectators are not affected by the excitation, their response in the phase domain is nil. Similarly, the noise signal is normally not correlated to the modulation excitation, and consequently the noise is also removed in the phase domain (for an infinite number of cycles). In practice, after a few cycles a quasi-steady state is reached, in which each following modulation give systematically the same response and an average over just a few modulations (typically 3 or 4) is enough to reach a sufficient signal.

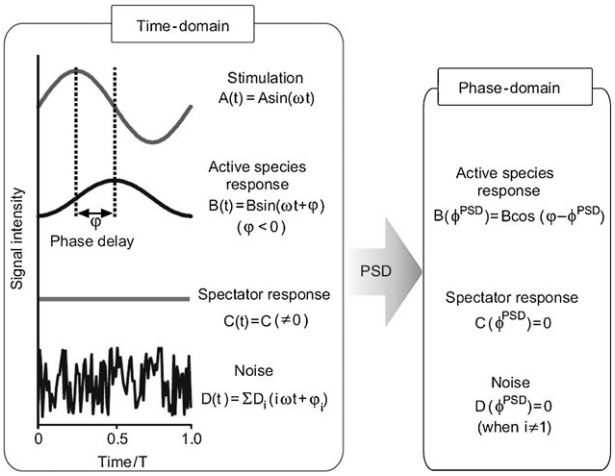

Fig. 9 Schematic illustration of sensitivity enhancement by phase-sensitive detection (PSD) (reproduce from ref. 49. Copyright 2008, with permission from Elsevier).

The delay between stimulation and response is linked to the kinetics, and comparing the delays between different molecules will help to gain insight into the mechanism of the process at the time scale studied. In the case of heterogeneous catalysis studied by ATR-FT-IR spectroscopy the frequency may be chosen from few fractions of a second to hours.

A clear limitation for the application of MES is that the system has to be reversible. A typical setup suitable for modulation excitation spectroscopy consisting of a flow cell with several inlet tubes is shown in Fig. 7. Modulation of the concentration of the liquid components is achieved by alternate opening and closing of the valves of the corresponding feed streams. In this case, the shape of the modulation excitation is approximately square and not sinusoidal. A tutorial review on the application of modulation excitation spectroscopy in heterogeneous catalysis has recently been published by Urakawa *et al.*[49]

5.5 Specific blocking of active sites

One of the main reasons of catalyst deactivation involves poisoning phenomena, *i.e.* a strong chemisorption of molecules on catalytic active sites.[50] Not always does poisoning lead to complete deactivation of the catalyst. When a catalyst exhibits several active sites, for example nanoparticles with extended faces, edges, and corners, the different active sites have generally different catalytic activities. The selectivity of a catalytic process can thus be improved by blocking (or poisoning) selectively some specific sites on the catalyst's surface. Furthermore selective poisoning (blocking) of active sites by a suitable blocking agent combined with *in situ* spectroscopy can serve as a powerful approach to elucidate the role of different sites on a catalytically active surface. The study of catalyst poisoning is a challenging task, nevertheless, *in situ* ATR-FT-IR together with theoretical spectrum calculation can provide the opportunity to follow directly the adsorbed species on different active sites. Thus, following a catalytic reaction with and without potential poisoning species (which are known to specifically block some active sites) can help to elucidate the specific contributions of

different surface sites to a reaction. Typical selective blocking agents involve CO, CO_2, NH_3 and pyridine.

5.6 Combination of ATR with other spectroscopic methods

While ATR-FT-IR spectroscopy is a powerful tool to analyze molecules adsorbed on solid surfaces, some other *in situ* spectroscopic techniques are providing complementary information about catalytic systems.[3] For instance, UV-vis spectroscopy has been utilized as a sensitive probe for metal particles in the case of Pd particles during ethanol oxidation.[51] A fast and reversible change in the UV-vis spectrum was observed during the switch from hydrogen to oxygen, which was attributed to changes in the optical properties of the Pd particles due to adsorption of hydrogen and oxygen. A slow and irreversible change in the UV-vis spectra was also monitored during oxidation as a result of oxygen flow and was associated to a change in Pd particle structure (oxidation state).

X-Ray absorption spectroscopy (XAS) is another powerful spectroscopic tool which can provide element-specific structural information on catalyst particles and especially the oxidation state of the metal under working conditions. Therefore, the combination of *in situ* ATR-FT-IR and XAS allows simultaneous monitoring of the surface species and the structure of the catalyst under working conditions. As an example, this combination has been used to follow the oxidation of alcohols over Pd/Al_2O_3.[52]

Another approach is the combination of different types of vibrational spectroscopies. As already introduced in Section 4.2, the information relating to each phase while working with multiphase catalytic systems is essential to identify the chemical processes. Thus, additional investigation of specific phases (liquid or gas) by means of IR or Raman simultaneously to the ATR-FT-IR spectra of the solid/liquid interface can provide crucial information to gain a better understanding of a catalytic system.[53]

6. Case studies

In order to illustrate the scope and potential of *in situ* ATR-FT-IR for probing solid/liquid interfaces, some selected studies are briefly presented here. For a more detailed consideration of these studies the reader is referred to the original articles. Various other examples can be found in a previous comprehensive review.[4]

6.1 Reactivity of supercritical CO_2 in the presence of hydrogen on noble metals

ATR-FT-IR was used to investigate *in situ* the reaction of CO_2 with H_2 under supercritical conditions over Pt, Pd, Rh and Ru on alumina under high pressure (up to 150 bar).[54] The aim was to clarify whether supercritical CO_2 is an inert solvent under typical hydrogenation conditions that is in the presence of a noble metal and hydrogen. The investigations showed that under typical hydrogenation conditions supercritical CO_2 can be considered as a rather inert solvent, but that it can undergo the reverse water-gas shift reaction: $CO_2 + H_2 \rightarrow CO + H_2O$. The formed CO can affect the noble metal by irreversible adsorption (blocking) on active sites, which in turn can influence the activity and selectivity of a particular hydrogenation process. The spectroscopic cell used for this investigation allowed to measure in ATR as well as in transmission mode. The cell has been described in Section 4.2. Catalyst films were prepared by PVD with typically 100 nm of Al_2O_3 deposited on ZnSe crystal followed by 1–2 nm of deposited noble metal. ATR-FT-IR spectra of absorbed CO on Pt, Rh, Pd and Ru under 5 bar of CO at 50 °C are presented in Fig. 10. Experiments on Rh, Pd and Pt showed signals corresponding to linear and bridge bonded CO. The signal intensity of bridge CO on Pt is much weaker than for Rh and Pd and centered at 1785 cm^{-1}. For Ru the only band of adsorbed CO was assigned to linear bonded species.[54] Fig. 10 also shows the evolution of the IR spectra under conditions where the reverse water gas shift reaction occurs. Molecular hydrogen cannot be detected since IR is not sensitive to H_2 vibration while CO_2 was easily detected at 2335 cm^{-1} (asymmetric O═C═O stretching mode) and also at 665 cm^{-1} (bending mode). The signals of absorbed CO at 2040 and 1859 cm^{-1} are slightly shifted compared to the spectra of pure CO under 5 bar. Bands at 3212 and 2863 cm^{-1} were assigned to OH and CH stretching bands, respectively. The positive signal at 3212 cm^{-1} is associated with a negative signal at *circa* 3500 cm^{-1} which was explained by a surface reorganization of the OH groups. Part of the CH signal was found to be correlated with other signals at 1457, 1351, 1100 cm^{-1} which were attributed to the presence of adsorbed oxygenated C_1 species (probably formate) on the catalyst surface.

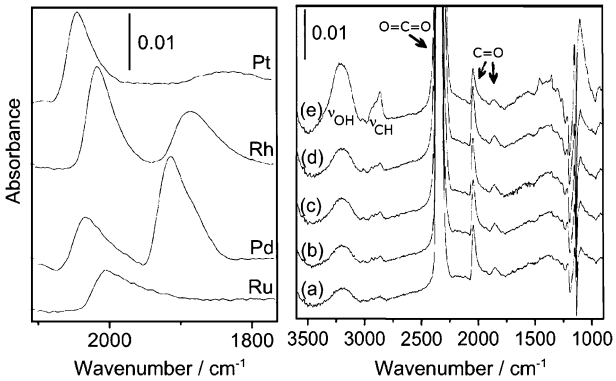

Fig. 10 (left) ATR-FT-IR spectra of the Al_2O_3-supported metal films in contact with CO under 5 bar of CO at 50 °C. (right) *In situ* ATR-FT-IR spectra corroborating that supercritical CO_2 can undergo reverse water gas shift reaction at 50 °C over Pt/Al_2O_3 in the presence of hydrogen (1 mol % H_2). Conditions: (a) 90 bar, (b) 100 bar, (c) 120 bar, (d) 140 bar, (e) 150 bar (adapted with permission from ref. 54. Copyright 2005, American Chemical Society).

6.2 Application of Greenler's surface selection rule and theoretical spectra calculation: adsorption of cinchonidine on Pt surface

A crucial issue for understanding asymmetric catalysis on chirally modified metals is to know how the chiral modifier is adsorbed on the catalytically active metal surface.[55] Fig. 11 shows the evolution of the ATR-FT-IR spectra of cinchonidine upon increase of its concentration on Pt/Al_2O_3 at 283 K and demonstrates that at a concentration of *circa* 3×10^{-5} M,

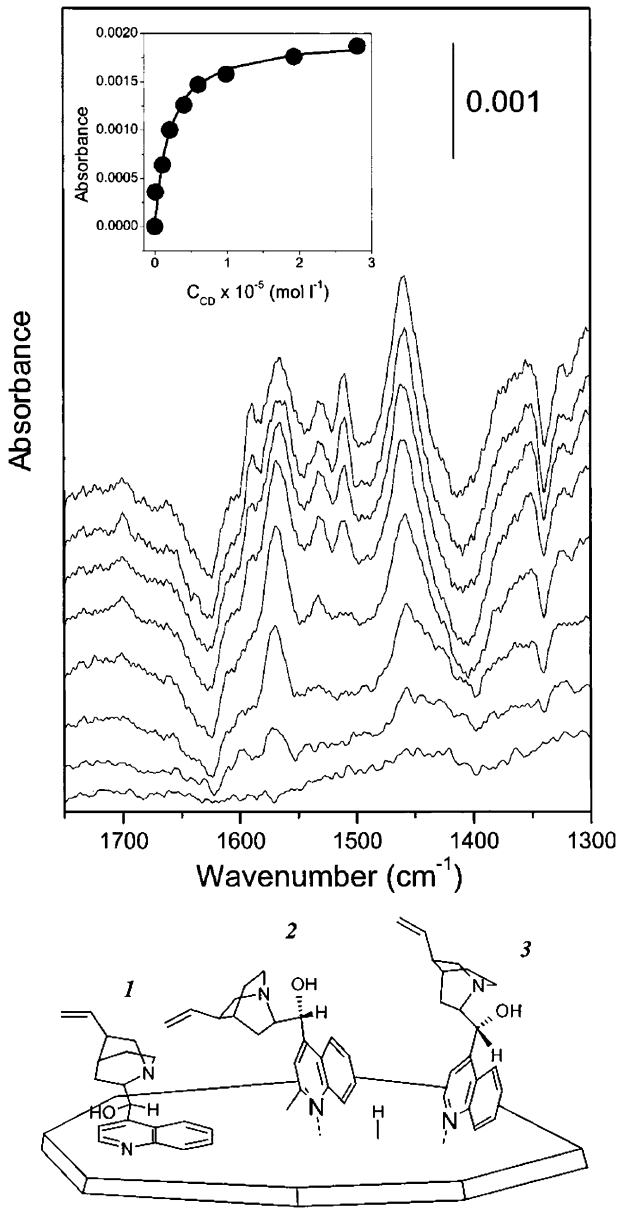

Fig. 11 (Top) ATR-FT-IR spectra of cinchonidine on Pt/Al_2O_3 at 283 K measured at increasing concentration (from 0 to 3×10^{-5} M) in CH_2Cl_2. The inset shows the absorbance of the 1458 cm^{-1} signal as a function of cinchonidine concentration. The signal at 1458 cm^{-1} is common to all adsorbed cinchonidine species. The inset indicates a Langmuir-type adsorption isotherm. On the bottom the proposed adsorption modes of cinchonidine on Pt/Al_2O_3 are schematically illustrated (adapted with permission from ref. 14. Copyright 2001, American Chemical Society).

nearly saturation coverage is reached. The evolution of the concentration of cinchonidine on the platinum surface (using the band at 1458 cm^{-1}, a common band for all possible adsorption modes) obeys a Langmuir adsorption isotherm. The negative bands at 1338, 1400, and 1625 cm^{-1} indicate the removal of ethylidyne (a decomposition product of the solvent CH_2Cl_2), and water from the interface.[14] The signals corresponding to the modifier can be classed into two groups: signals at 1511 and 1590 cm^{-1} progressively increase with concentration, while the signals at 1530 and *ca.* 1570 cm^{-1} decrease slightly for the highest concentrations. Three possible geometries of cinchonidine on Pt/Al_2O_3 have been determined after a careful analysis of IR spectra at each concentration, IR spectra of reference compounds, and quantum chemistry calculations. These geometries are also depicted in Fig. 11. Using these assignments and Greenler's surface selection rule[43,44] the following picture emerged. At low concentration, the band at 1570 cm^{-1} increases rapidly, which corresponds to the "flat" orientation (**1**) where the aromatic quinoline ring lies nearly parallel to the metal surface. At higher concentration, bands at 1590 and 1511 cm^{-1} are appearing, indicating that the two others orientations (**2** and **3**) become favored.[14]

6.3 Modulation excitation spectroscopy: Knoevenagel condensation

ATR-FT-IR in combination with MES was successfully applied for elucidating the liquid-phase Knoevenagel condensation between benzaldehyde and ethyl cyanoacetate on aminopropyl-modified silica as catalyst coated on a ZnSe IRE.[25] Experiments were performed under solvent and solvent-less conditions, as well as in flow and static modes, with reactant(s), and/or product, and/or catalyst, in order to access each reaction step involved in the reaction. After careful analysis of each experiment, the mechanism shown in Scheme 1 could be derived. The formation and consumption of the reaction intermediate **5** (benzaldimine) was observed *in situ via* IR

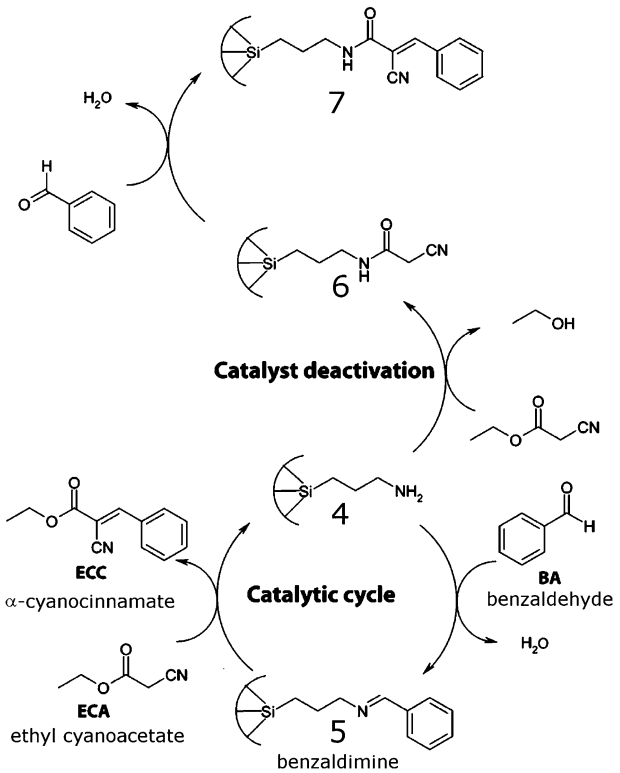

Scheme 1 Mechanism of the Knoevenagel reaction between benzaldehyde and ethyl cyanoacetate on aminopropyl-modified silica and additional reactions possibly leading to catalyst poisoning (adapted with permission from ref. 25. Copyright 2006, American Chemical Society).

spectroscopy, which supported the proposed mechanism. Benzaldimine is formed by the reaction of benzaldehyde over the catalyst, and is consumed by the reaction with ethyl cyanoacetate to form the ethyl cyanoacetate. Apart from understanding the catalytic cycle, one of the reactants (ethyl cyanoacetate) was found to be responsible for some apparent catalyst poisoning, as illustrated in Scheme 1. This catalyst deactivation is very slow compared to the benzaldimine formation. In this example, the intermediate bonded to the catalyst could only be detected directly by *in situ* observation.

MES experiments were completed in the quasi-steady state which was reached after three periods. 60 spectra were recorded during each modulation period which was around six minutes. Each spectrum was obtained by FT of an average of 60 interferograms and the spectra were averaged over three cycles. The concentration MES approach reveals synchronization between the decrease of concentration of the intermediate and the increase of the product concentration. The concentration MES of both reactants over the catalyst is shown in Fig. 12. The bands at 1645 and 1647 cm^{-1} are due to the intermediate of the reaction in toluene and cyclohexane, respectively. In the first half of the modulation, the first reactant benzaldehyde (BA) is flown over the catalyst, which induces an increase of the concentration of the intermediate, while during the second half, the intermediate is reacting with the second reactant ethyl cyanoacetate (ECA) to form the product α-cyanocinnamate (ECC). This MES experiment corroborated the findings obtained with a series of static and stop flow IR experiments. The benefit of the modulation experiments is the easy comparison of the kinetics under catalytic working conditions, despite the small IR signal (inset of Fig. 12). The concentration MES performed with toluene and cyclohexane as solvent demonstrates a different behavior of the intermediate. The formation and consumption of the intermediate was faster in cyclohexane than in toluene which correlates well with the fact that the catalyst was more active in cyclohexane.

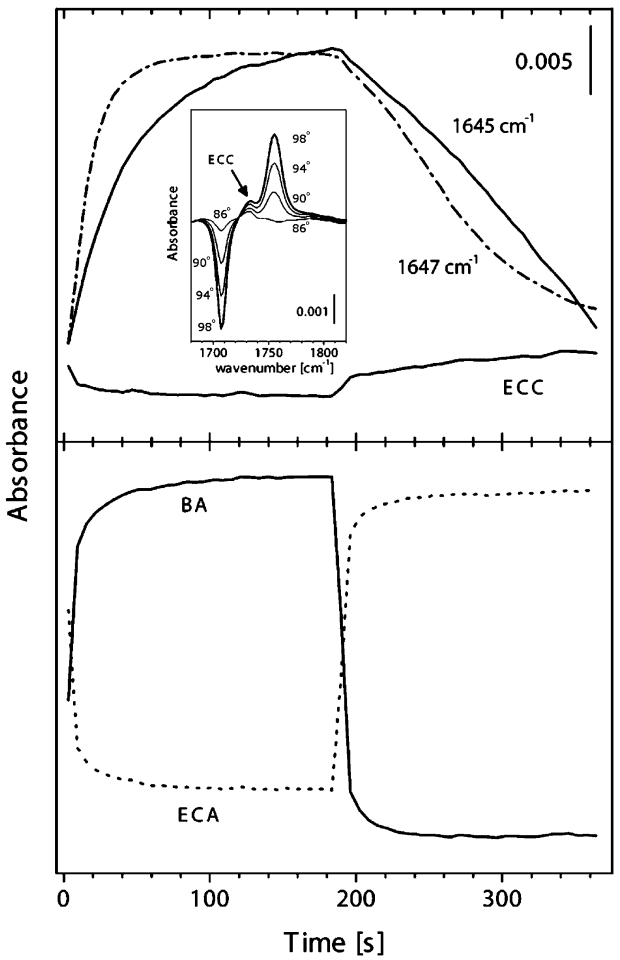

Fig. 12 Time dependence of the signals at (top) 1645 (bold line) and 1734 cm^{-1}, and (bottom) 1707 and 1757 cm^{-1} of the corresponding benzaldehyde (BA) *vs.* ethyl cyanoacetate (ECA) concentration modulation experiments in toluene averaged over three modulation cycles. The inset shows selected phase-resolved spectra in the 1820–1680 cm^{-1} spectral region demodulated in the range of phase angles 86°–98° (bold = 98°). The dashed–dotted line in the top panel represents the behavior of the benzaldimine signal at 1647 cm^{-1} in an identical experiment performed in cyclohexane. Conditions: $C_{BA} = C_{ECA} = 20$ mM; 60 °C (reprinted with permission from ref. 25. Copyright 2006, American Chemical Society).

Various other successful applications of ATR combined with MES can be found in the literature.[24,56–58] More recently the scope of MES has been extended to absolute configuration modulation for investigating chiral interfaces.[59–61]

6.4 Specific site blocking: nature of active sites in palladium-catalyzed alcohol oxidation of benzyl alcohol

The application of *in situ* ATR-FT-IR spectroscopy in combination with specific site blocking proved to be a powerful approach for unraveling the role of the Pd surface sites with different coordination in the aerobic oxidation of benzyl alcohol over a Pd/alumina catalyst. Not only reactant and main product could be detected, but also benzoic acid which was undetectable in the reaction mixture by GC analysis because it accumulated on the surface of the alumina support.[23] CO was used as a selective blocking agent. Various IR bands of CO absorbed on Pd/Al_2O_3 were discernible. The most interesting signal appeared at 1968 cm^{-1} and corresponds to bridge CO on (100) planes and defect sites (edges, corners). The signal slightly below 1968 cm^{-1}, indicated the population of hollow sites on (111) planes, and the band at 2074 cm^{-1} was associated with linear CO on defect sites.[62] The time dependence of the bands indicative of bridge CO and benzaldehyde of a solution of benzyl alcohol brought in contact with Pd/alumina under Ar and after pre-equilibration with CO is shown Fig. 13a. The correlation between the sudden appearance of the signal due to benzaldehyde and the depletion of the CO signal at 1968 cm^{-1} shows the interdependence between the benzaldehyde formation and the blocking of active sites by bridge CO.[62,63] The experiment reveals that the alcohol oxidation was inhibited as long as CO remained on bridge sites of the catalyst (defects, corner and edges and most likely on (100) planes) as presented in Fig. 13b. Together with other IR experiments,[62,63] it was found that the dehydrogenation (oxidation) of benzyl alcohol occurs on all faces exposed by the Pd particles while the subsequent decomposition to CO and benzene occurs mainly on (111) faces.

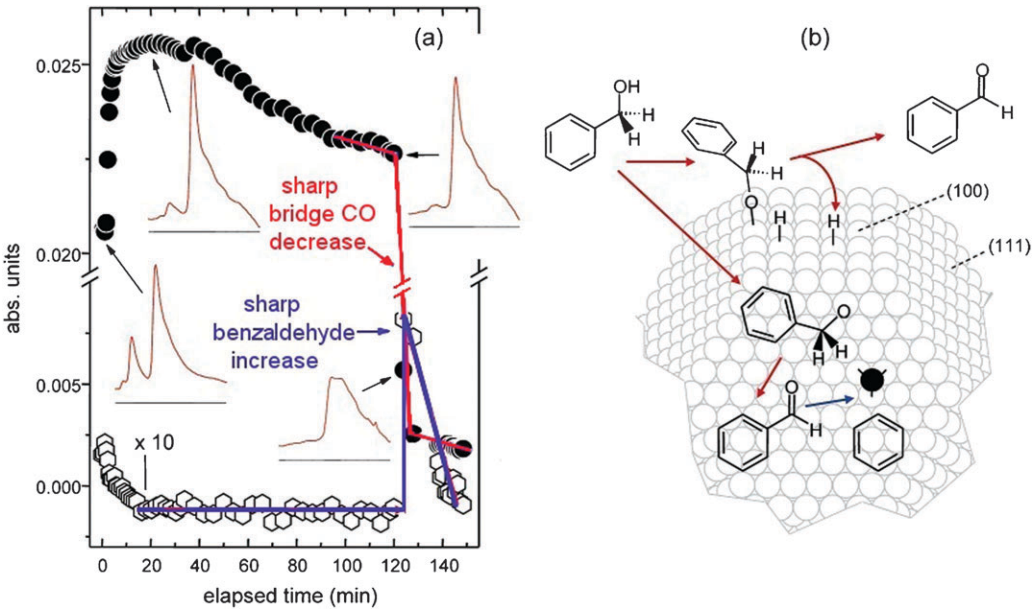

Fig. 13 (a) Time dependence of the signal of bridge CO (initially at 1968 cm^{-1}, filled circles) and of benzaldehyde (1713 cm^{-1}, diamonds, 10 times magnified) when admitting a solution of benzyl alcohol under Ar on Pd/Al_2O_3 pre-equilibrated with CO. Insets depict snapshots of the CO signals in the range of 2100–1800 cm^{-1}. Red and blue lines were added to help the reader to follow signal from bridge CO and benzaldehyde, respectively. (b) Artist view on the structural dependence of the oxidative dehydrogenation of benzyl alcohol on an ideal cuboctahedron Pd crystallite. Alcohol dehydrogenation occurs on all Pd sites (red arrows), whereas product decomposition occurs predominantly on (111) planes (blue arrow). Only dehydrogenation on edges and (111) planes is represented for clarity. The black dot represents CO on hollow sites (top view) (adapted with permission from ref. 62. Copyright 2006, American Chemical Society).

Interestingly, a similar selective poisoning of the Pd/Al_2O_3 catalyst was later realized by adding bismuth as a promoter.[63] When Bi was deposited on Pd particles, the selectivity of the reaction improved considerably while the carbon monoxide IR signal decreased significantly, as shown in Fig. 14. The yield of the reaction could be estimated directly by IR as the benzaldehyde concentration could be followed using the sharp band at 1713 cm^{-1}, while the CO adsorbed on Pd exhibited a signal at 1950 cm^{-1} and a broad band centered at 1850 cm^{-1}. The promoting effect of Bi can be interpreted as blocking of sites present on Pd (111) planes. Since the side reaction occurs on the (111) planes of Pd, as demonstrated by the experiments with the CO active site blocking, the addition of Bi is beneficial for the selectivity to benzaldehyde.

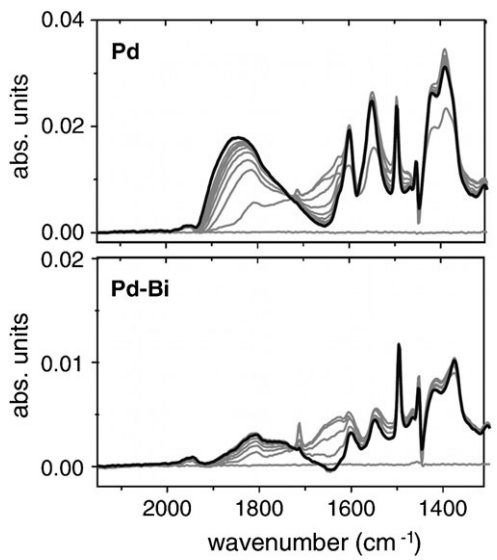

Fig. 14 ATR-FT-IR spectra taken during benzyl alcohol oxidation on 5 wt% Pd/Al_2O_3 (Pd) and 0.75 wt% Bi–5 wt% Pd/Al_2O_3 (Pd–Bi). Black line corresponds to last spectrum. (Reprinted from ref. 63. Copyright 2005, with permission from Elsevier).

For the same catalytic reaction catalyzed by supported Au nanoparticles, thiols have also proven their potential for selectively blocking catalytic sites. The ratio of the intensity of the IR bands ($\nu_{(S-H)}/\nu_{(C=O)}$) indicated that the blocking agent is adsorbed *via* the thiol group in the case of mercaptoacetic acid (MAA).[26] DFT calculations of the adsorption energy of MAA on Au with multiple adsorption sites confirmed the analysis of the IR spectra, since the best adsorbed configuration was found to be between the thiol group and the edge between Au (111) and (100) facets.[26] MAA is thus selectively blocking the edges of Au nanoparticles while another thiol, *n*-octadecanethiol (ODT), was found to bind preferably on Au facets. The comparison of the catalytic activity of Au for the hydrogenation of ketopantolactone and the oxidation of benzyl alcohol, using both thiols as blocking agent, lead to the conclusion that the carboxyl group hydrogenation is mainly occurring on corners or edges, while benzyl alcohol is preferentially oxidized on facets.

7. Potential, limitations, and challenges

ATR-FT-IR spectroscopy is probably presently the most used technique for probing *in situ* solid/liquid interfaces of catalytic systems. The advantage of infrared (and Raman) spectroscopy

is the sensitivity to molecular interactions, and when properly applied the ATR mode is probing specifically the interface (surface) region where heterogeneous catalysis occurs. ATR-FT-IR can provide important information about chemical and geometrical structures of catalytic interfaces as well as on reaction mechanisms and kinetics. The difficulty of differentiating between the active and spectator molecules of the catalytic reaction is nevertheless still a challenge, but transient experiments and MES combined with phase sensitive detection proved to be promising for discriminating between active and spectator species. Beside this common problem, some molecules (diatomic homonuclear molecules such as H_2, O_2, N_2 or halogens) are not active in IR spectroscopy. Note that the presence of a dissolved gas in a liquid can induce effects that can change the IR spectrum due to reflectivity changes of the liquid. However, the interpretation of such changes is difficult, as similar effects can also be caused by alteration of the reflectivity of the solid material due to surface oxidation or reduction.[64] Another approach, as IR spectroscopy is not sensitive to all chemicals, is to use a complementary technique combined with ATR-FT-IR to obtain a better insight in the catalytic system. Raman spectroscopy can be used to observe diatomic homonuclear molecules, and X-ray absorption spectroscopy is able to probe the state of the metal nanoparticles under working conditions.

Using ATR-FT-IR spectroscopy, the depth profile (from *circa* 0.2 to 2 μm) can be obtained either by analyzing the intensity of bands at different wavelengths, or by using the same band with different incident angle.[65]

By using infrared array detectors instead of a single infrared detector, IR images of the sample on the IRE can be obtained. This gives access to high-throughput screening by coating several catalysts on the same IRE (which allows a more precise screening as the reaction conditions are identical), or by analysis of a solid/liquid interface of the same catalyst film with many different solutions separated from each other by a grid previously coated on the IRE. This methodology has already proven to be efficient, for example, in polymer science.[66]

For the specific studies of chiral molecules other methods, such as vibrational circular dichroism (VCD), could be preferable over the standard ATR technique. VCD is the differential absorption of left- and right-circularly polarized infrared light by chiral molecules.[67] VCD has been successively applied to elucidate the conformation and binding sites of cinchona alkaloids and similar chiral modifiers with carboxylic acids.[68] This study indicated that binding of a non-chiral carboxylic acid to the alkaloid induces VCD in vibrations associated with the acid. Observation of this induced VCD allows probing of the chiral binding site. Other infrared spectroscopy techniques which use polarized IR light, such as polarization modulation infrared reflection absorption spectroscopy (PM-IRRAS), have also been applied recently to study heterogeneous catalytic reactions in solid/liquid systems.[69–71] Briefly, PM-IRRAS uses the different behavior of perpendicular and parallel polarized light at the metal surface while the light reflects on it. By comparing both polarizations it is possible to observe specifically the molecules at the interface with the metal surface. In PM-IRRAS, the IR light needs to travel through the sample, as in transmission mode, which unfortunately restricts the potential of this technique to *in situ* solid/liquid interface studies. Nevertheless, using techniques based on polarized light will probably provide substantial further insight in chemical processes occurring at catalytic solid/liquid interfaces.

Commercially available immersion probes have made the ATR technique easily applicable, particularly for research on homogeneous liquid systems. It can be expected that the versatility and possibilities of ATR-FT-IR will be further extended by the development of new high-transmitting fibre optic materials and technical innovations in ATR hardware and IR-instrumentation.

Acknowledgements

AB thanks past and present co-workers for their valuable contributions, their enthusiasm and perseverance, which have greatly stimulated our research on *in situ* spectroscopy.

References

1 R. P. Eischens, W. A. Pliskin and S. A. Francis, *J. Chem. Phys.*, 1954, **22**, 1786–87.
2 R. P. Eischens and W. A. Pliskin, *Adv. Catal.*, 1958, **10**, 1–56.
3 B. M. Weckhuysen, *In situ Spectroscopy of Catalysts*, American Scientific Publishers, San Diego, 2004.
4 T. Bürgi and A. Baiker, *Adv. Catal.*, 2006, **50**, 227–283.
5 J. Ryczkowski, *Catal. Today*, 2001, **68**, 263–381.
6 C. J. Hirschmugl, *Surf. Sci.*, 2002, **500**, 577–604.
7 P. R. Griffiths and J. A. de Haseth, *Fourier Transform Infrared Spectrometry*, John Wiley & Sons, New York, 1986.
8 K. Krishnan, in *Fourier Transform Infrared Spectroscopy; Applications to Chemical Systems*, ed. J. R. Ferraro and L. J. Basile, Academic Press, Orlando, FL, 1985.
9 T. Visser, *In situ Attenuated Total Reflection Infrared Spectroscopy of Catalysts*, ed. B. M. Weckhuysen, in *In situ Spectroscopy of Catalysts*, American Scientific Publishers, San Diego, 2004, pp. 47–58.
10 H. B. Mark and B. S. Pons, *Anal. Chem.*, 1966, **38**, 119–121.
11 W. N. Hansen, T. Kuwana and R. A. Osteryou, *Anal. Chem.*, 1966, **38**, 1810–1821.
12 K. Kunimatsu, *J. Electroanal. Chem.*, 1982, **140**, 205–210.
13 D. Ferri, T. Bürgi and A. Baiker, *J. Phys. Chem. B*, 2001, **105**, 3187–3195.
14 D. Ferri and T. Bürgi, *J. Am. Chem. Soc.*, 2001, **123**, 12074–12084.
15 I. Ortiz-Hernandez and C. T. Williams, *Langmuir*, 2003, **19**, 2956–2962.
16 G. M. Hamminga, G. Mul and J. A. Moulijn, *Chem. Eng. Sci.*, 2004, **59**, 5479–5485.
17 R. He, R. R. Davda and J. A. Dumesic, *J. Phys. Chem. B*, 2005, **109**, 2810–2820.
18 S. D. Ebbesen, B. L. Mojet and L. Lefferts, *Langmuir*, 2006, **22**, 1079–1085.
19 N. J. Harrick, *Phys. Rev. Lett.*, 1960, **4**, 224–226.
20 J. Fahrenfort, *Spectrochim. Acta*, 1961, **17**, 698–709.
21 D. L. Doak and J. A. Phillips, *Biotechnol. Prog.*, 1999, **15**, 529–539.
22 W. D. Sproul, *Surf. Coat. Technol.*, 1996, **81**, 1–7.
23 C. Keresszegi, D. Ferri, T. Mallat and A. Baiker, *J. Phys. Chem. B*, 2005, **109**, 958–967.
24 T. Bürgi and A. Baiker, *J. Phys. Chem. B*, 2002, **106**, 10649–10658.
25 R. Wirz, D. Ferri and A. Baiker, *Langmuir*, 2006, **22**, 3698–3706.
26 P. Haider, A. Urakawa, E. Schmidt and A. Baiker, *J. Mol. Catal. A: Chem.*, 2009, **305**, 161–169.
27 B. J. Ninness, D. W. Bousfield and C. P. Tripp, *Appl. Spectrosc.*, 2001, **55**, 655–662.
28 D. Rivera, P. E. Poston, R. H. Uibel and J. M. Harris, *Anal. Chem.*, 2000, **72**, 1543–1554.

29 C. Keresszegi, D. Ferri, T. Mallat and A. Baiker, *J. Catal.*, 2005, **234**, 64–75.
30 M. M. Braun and L. Pilon, *Thin Solid Films*, 2006, **496**, 505–514.
31 R. F. Aroca, D. J. Ross and C. Domingo, *Appl. Spectrosc.*, 2004, **58**, 324A–338A.
32 B. Panella, A. Vargas, D. Ferri and A. Baiker, *Chem. Mater.*, 2009, **21**, 4316–4322.
33 F. Jutz, J.-D. Grunwaldt and A. Baiker, *J. Mol. Catal. A: Chem.*, 2008, **279**, 94–103.
34 T. Seki, J. M. Andanson, F. Jutz and A. Baiker, *Appl. Spectrosc.*, 2009, **63**, 1008–1014.
35 M. S. Schneider, J. D. Grunwaldt, T. Bürgi and A. Baiker, *Rev. Sci. Instrum.*, 2003, **74**, 4121–4128.
36 A. Urakawa, R. Wirz, T. Bürgi and A. Baiker, *J. Phys. Chem. B*, 2003, **107**, 13061–13068.
37 D. Ferri, T. Bürgi and A. Baiker, *Helv. Chim. Acta*, 2002, **85**, 3639–3656.
38 G. Mul, G. M. Hamminga and J. A. Moulijn, *Vib. Spectrosc.*, 2004, **34**, 109–121.
39 S. A. Tromp, G. Mul, Y. Zhang-Steenwinkel, M. T. Kreutzer and J. A. Moulijn, *Catal. Today*, 2007, **126**, 184–190.
40 F. Hoxha, L. Königsmann, A. Vargas, D. Ferri, T. Mallat and A. Baiker, *J. Am. Chem. Soc.*, 2007, **129**, 10582–10590.
41 B. Behzadi, A. Vargas, D. Ferri, K.-H. Ernst and A. Baiker, *J. Phys. Chem. B*, 2006, **110**, 17082–17089.
42 J. M. Delgado, R. Blanco, J. M. Orts, J. M. Perez and A. Rodes, *J. Phys. Chem. C*, 2009, **113**, 989–1000.
43 R. G. Greenler, *J. Chem. Phys.*, 1966, **44**, 310–315.
44 R. G. Greenler, D. R. Snider, D. Witt and R. S. Sorbello, *Surf. Sci.*, 1982, **118**, 415–428.
45 R. G. Brereton, *Analyst*, 2000, **125**, 2125–2154.
46 G. M. Escandar, N. K. M. Faber, H. C. Goicoechea, A. M. de la Pena, A. C. Olivieri and R. J. Poppi, *TrAC, Trends Anal. Chem.*, 2007, **26**, 752–765.
47 J.-M. Andanson, F. Jutz and A. Baiker, *Appl. Spectrosc.*, 2010, **64**, 286–292.
48 F. Jutz, J. M. Andanson and A. Baiker, *J. Catal.*, 2009, **268**, 356–366.
49 A. Urakawa, T. Bürgi and A. Baiker, *Chem. Eng. Sci.*, 2008, **63**, 4902–4909.
50 C. H. Bartholomew, *Appl. Catal., A*, 2001, **212**, 17–60.
51 T. Bürgi, *J. Catal.*, 2005, **229**, 55–63.
52 C. Mondelli, D. Ferri, J.-D. Grunwaldt, F. Krumeich, S. Mangold, R. Psaro and A. Baiker, *J. Catal.*, 2007, **252**, 77–87.
53 M. Caravati, J.-D. Grunwaldt and A. Baiker, *Phys. Chem. Chem. Phys.*, 2005, **7**, 278–285.
54 M. Burgener, D. Ferri, J.-D. Grunwaldt, T. Mallat and A. Baiker, *J. Phys. Chem. B*, 2005, **109**, 16794–16800.
55 A. Baiker, *J. Mol. Catal. A: Chem.*, 1997, **115**, 473–493.
56 A. Gisler, T. Burgi and A. Baiker, *Phys. Chem. Chem. Phys.*, 2003, **5**, 3539–3548.
57 A. Gisler, T. Burgi and A. Baiker, *J. Catal.*, 2004, **222**, 461–469.
58 N. Bonalumi, T. Burgi and A. Baiker, *J. Am. Chem. Soc.*, 2003, **125**, 13342–13343.
59 R. Wirz, T. Bürgi and A. Baiker, *Langmuir*, 2003, **19**, 785–792.
60 R. Wirz, T. Bürgi, W. Lindner and A. Baiker, *Anal. Chem.*, 2004, **76**, 5319–5330.
61 R. Wirz, D. Ferri and A. Baiker, *Anal. Chem.*, 2008, **80**, 3572–3583.
62 D. Ferri, C. Mondelli, F. Krumeich and A. Baiker, *J. Phys. Chem. B*, 2006, **110**, 22982–22986.
63 D. Ferri and A. Baiker, *Top. Catal.*, 2009, **52**, 1323–1333.
64 T. Bürgi, R. Wirz and A. Baiker, *J. Phys. Chem. B*, 2003, **107**, 6774–6781.
65 K. R. Kirov and H. E. Assender, *Macromolecules*, 2005, **38**, 9258–9265.
66 K. L. A. Chan and S. G. Kazarian, *J. Comb. Chem.*, 2005, **7**, 185–189.
67 M. Bieri, C. Gautier and T. Bürgi, *Phys. Chem. Chem. Phys.*, 2007, **9**, 671–685.
68 T. Bürgi, A. Vargas and A. Baiker, *J. Chem. Soc., Perkin Trans. 2*, 2002, 1596–1601.
69 D. M. Meier, A. Urakawa, R. Mader and A. Baiker, *Rev. Sci. Instrum.*, 2009, **80**, 094101–1-11.
70 D. M. Meier, A. Urakawa and A. Baiker, *J. Phys. Chem. C*, 2009, **113**, 21849–21855.
71 D. M. Meier, A. Urakawa and A. Baiker, *Analyst*, 2009, **134**, 1779–1780.

